PROCEEDINGS OF SCIENCE

A Fermi-LAT view of the sky below 100 MeV

Thibaut Desgardin[*†]
Laboratoire Univers et Particules de Montpellier (LUPM)
E-mail: thibaut.desgardin@univ-montp2.fr

The Large Area Telescope (LAT) collaboration has recently completed the development of the "Pass 8" event-level analysis that provides a comprehensive revision of the algorithms used for event reconstruction and particle identification. Among other performance improvements, Pass 8 provides a drastic increase in the effective area of the LAT instrument below 100 MeV. Together with a better modelling of the instrument's energy response function, Pass 8 gives us the opportunity to look with the LAT at the largely unexplored 10-100 MeV energy regime. In this proceeding we will summarize the main technical improvements and show preliminary science results obtained below 100 MeV

The 34th International Cosmic Ray Conference,
30 July- 6 August, 2015
The Hague, The Netherlands

[*]Speaker.
[†]on behalf of the Fermi Large Area Telescope collaboration

PoS(ICRC2015)839

1. Introduction

After 7 years in orbit the Large Area Telescope (LAT) has provided a wealth of data on the gamma-ray sky spanning the energy range from 20 MeV to more than 300 GeV. Due to the technical challenges associated with modelling the instrument response functions and backgrounds at lower energies, most LAT analyses start at 100 MeV. As part of the effort by the LAT team to improve the capabilities of the instrument, work is on-going to enable analyses of LAT data below 100 MeV. The Pass 8 event analysis plays a major role in this direction by improving the instrument performance at low energies and providing a more accurate parameterization for the LAT energy dispersion response function. In this paper we will present these new improvements and we will show the effect on data analysis.

2. The low energy energy regime of the LAT

2.1 The Large Area Telescope

The LAT has been designed to study the gamma-ray sky from 20 MeV to over 300 GeV. Photons in this energy range cannot be focused: they interact mainly via pair production. The LAT uses the resulting electron-positron pair to reconstruct the energy and direction of the incident photon. To do so, the LAT relies on 3 main subsystems: a tracker-converter subsystem (**TKR**) made of silicon strip detector planes interleaved with tungsten foils to enhance photon interaction probability; an electromagnetic calorimeter (**CAL**), that is located below the tracker to absorb part of the shower and measure the gamma-ray energy; and an anti-coincidence detector (**ACD**), made of plastic scintillator tiles, covers the tracker and provides a veto signal to separate neutral from charged particles. The LAT employs a modular design based on individual "towers" that each contain a TKR and a CAL module. A 4 x 4 array of towers are kept together by an aluminium grid (the main mechanical structure). The reconstruction of photon information such as energy and incoming direction is processed from each subsystem's data on the secondary charged particles via the event analysis framework named Pass 8 [1] .

2.2 Technical improvements

2.2.1 Pass 8 in a nutshell

Previous LAT event-level analyses were based on reconstruction algorithms largely developed before launch using Monte Carlo simulations in a series of iterations that we call Passes: Pass 6 was released at launch and was followed in August 2011 by Pass 7 [2], which mitigated the impact of some of the limitations of its predecessor. On-orbit experience with the fully integrated detector has revealed some neglected or overlooked issues: primarily the effect of chance coincidences with cosmic rays (that we call Ghost Events). Clear improvements, with the potential to greatly extend the LAT science capabilities, have been identified in three main areas: the Monte Carlo simulation of the detector, the event reconstruction and the background rejection. Event selections for science analysis were also developed and used for the study of possible systematic effects and the assessment of their uncertainties. One of the goals of the Pass 8 effort is in fact to reduce systematic uncertainties in the instrument response function (usually produced via simulations and

corrected, if necessary, with flight data). The Pass 8 acceptance is compared with the current one in figure 1. We find a ~25% increase between 1 and 30 GeV, while at low energy (< 100 MeV) the increase can be a factor 2 or more. Monte Carlo predictions are confirmed by an analysis of flight data from the Crab pulsar (data points are shown in bottom panel of figure 1).

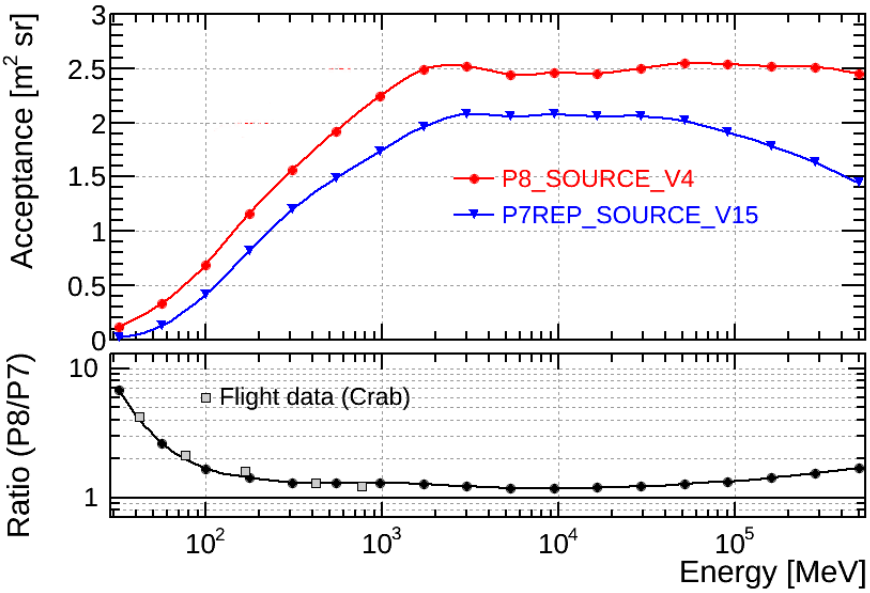

Figure 1: Comparison of new (Pass 8 in red) and current (Pass 7 in blue) performance of the event selection recommended for gamma-ray source analysis. The top plot shows the acceptance as a function of the energy, while the bottom plot shows the Pass 8/Pass 7 acceptance ratio (black points). The measured acceptance ratio (gray squares) is evaluated with an analysis of flight data from the Crab Pulsar and confirms the Monte Carlo prediction.

2.2.2 The LAT new energy dispersion parametrisation

In the low energy regime it is often found that the electron from the pair conversion does not reach the calorimeter, hence making energy reconstruction more complicated. The TKR can nevertheless be used to reconstruct the incoming photon energy but is less accurate than the calorimeter. This implies that energy dispersion is more important at low energy, and should be taken into account in the analysis. However, Monte Carlo studies showed that the parametric function used to model energy dispersion was not accurate enough at low energy [6]. A new function was then devised to fix this issue.

The energy dispersion of the LAT is defined in terms of the fractional difference between the reconstructed energy (E') and the true energy (E) of the events:

$$\frac{\delta E}{E} = \frac{E' - E}{E} \tag{2.1}$$

The energy dispersion parameterization is fit independently in two-dimensional bins in true energy (E) and incidence angle (θ). The default binning for the energy dispersion parameterization is 4 energy bins per decade, from 0.75 to 6.50 in log(Energy) (corresponding to the range 5.6 MeV

to 3.2 TeV), and 8 angle bins, equally spaced from 0.2 to 1.0 in cos(θ). For each bin, a scaled energy dispersion is calculated, binned into a histogram, and then fitted as described below. First, we define

$$x = \frac{\delta E}{E S_D(E,\theta)} \tag{2.2}$$

where the scaling factor depends on both true energy (E) and true incidence angle (θ) and ensures that the distributions do not vary to much from a bin to another. :

$$S_D(E,\theta) = c_0(logE)^2 + c_1(\cos\theta)^2 + c_2 logE + c_3\cos\theta + c_4 logE\cos\theta + c_5 \tag{2.3}$$

The scaling factor is derived from the 68% containment of the unscaled energy distribution in each bin. It is then modelled by the above function. All 6 parameters have distinct values for different event types. A new energy dispersion parameterization has been developed in conjunction with the Pass 8 development. The new parameterization is a combination of 2 asymmetric exponential power functions normalized to unity. The explicit expression for the asymmetric exponential power function (g) is:

$$g(x;\sigma,k,b,p) = \frac{p}{\sigma\Gamma(1/p)}\frac{1}{1+k^2}\begin{cases} \exp\left(-\frac{k^p}{\sigma^p}|x-b|^p\right) & \text{if } x-b \geqslant 0 \\ \exp\left(-\frac{1}{k^p\sigma^p}|x-b|^p\right) & \text{if } x-b < 0 \end{cases} \tag{2.4}$$

were σ is the "width" of the function, k is the skewness parameter, b the bias and p the exponential index. The final energy dispersion function combines two asymmetric exponential power functions with overall normalization equal to one. To do so we introduce an additional parameter (F) which is the fraction of events in the first asymmetric exponential power function. The full energy dispersion function is thus given by:

$$D(x) = F \times g(x;\sigma_1,k_1,b_1,p_1) + (1-F)\times g(x;\sigma_2,k_2,b_2,p_2) \tag{2.5}$$

Hence the final function depends on 9 parameters: F, σ_1, k_1, b_1, p_1, σ_2, k_2, b_2, p_2. The plot on figure 2 shows a histogram of the scaled energy dispersion for simulated events passing the Pass 8 SOURCE class and the FRONT conversion type. The best-fit energy dispersion function, shown superimposed as the solid black curve, gives a better result than the best-fit with the previous energy dispersion parametrisation, shown superimposed as the dotted black curve, especially at very low and very high energies.

3. Preliminary studies at low energy

In this section we will present the first results on low energy (E<100MeV) gamma-ray with the LAT. We used a tool named GaRDiAn [5], which allows us to fit the full sky using the HEALPix[1] framework.

We considered 6 years of Pass 8 data belonging to the ultracleanveto class, designed to mitigate particle background contamination; with reconstructed energies between 10 MeV and 1 GeV; with zenith angles $\leq$ 105 degreees; and used the P8R2_ULTRACLEANVETO_V6 instrument response functions. We also removed data during LAT-detected gamma-ray bursts and solar flares.

[1] http://healpix.jpl.nasa.gov/

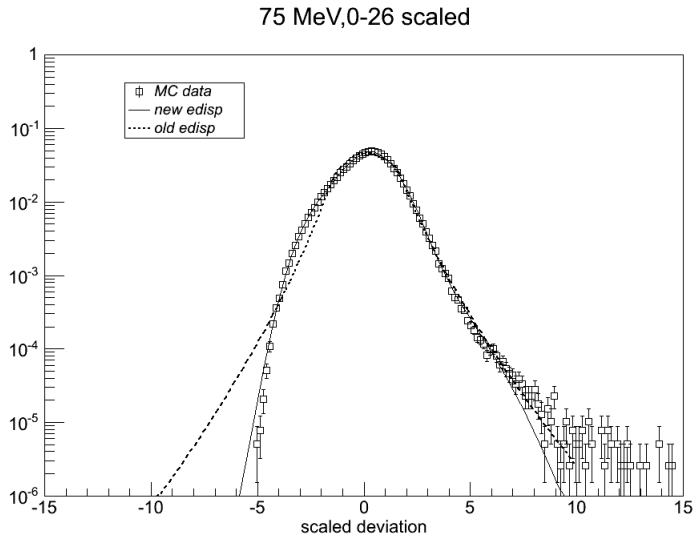

Figure 2: Histogram of the scaled energy dispersion fitted by the new energy dispersion response function parametrisation (solid black line) and the previous one (black dotted line). The histogram was generated through Monte Carlo simulation, after applying the SOURCE class cuts. It only contains events with true energy in the bin centered on 75 MeV and true θ between 0 and 26 degrees.

3.1 Diffuse model

The diffuse models provided by the collaboration to the public do not cover the energy range of the data. For the Galactic diffuse model and sun/moon emission model, we extrapolated down to 10 MeV, since the morphology does not change significantly with decreasing energy for these sources. We extrapolated the average SED, but kept the spatial structure fixed to that of the lowest energy bin in the released model. For the Earth limb emission model, which is one of the most prominent components at low energy, the morphology varies too much with decreasing energy to simply extrapolate the spectrum down as was done for the other components. We decided to use a similar procedure to the one used by the LAT collaboration to derive the Earth limb template *i.e.* we used a declination (DEC) ring model. The main differences in our approach are: we use the DEC ring model to account for both earth limb and isotropic emission and when we fit to data, we fit bin by bin.

Now that we know how to proceed to model each emission component (Galactic diffuse, earth-limb, isotropic, sun/moon), we can fit these models to our dataset. To do that we fixed all the sources from the 3FGL catalogue [3]. The methodology consists of a bin by bin fit of the prefactor of each model. We used 10 bins per decade between 10 MeV and 1 GeV.

In a second iteration, now that the morphology of the Earth limb is known, we free some sources to check their low energy behaviour. We did this for 39 bright sources visible in the counts map and we present the results for two of them (Vela and Crab) in the following section

3.2 Results on point sources

The fit of the sources was made in a bin by bin fashion. In each bin the source is considered to be a power law (see eq. 3.1) of fixed index $\gamma = -2$. Then we fit a prefactor (N_0) to this power-law

spectrum in each bin. As before we used 10 bins per decade between 10 MeV to 1 GeV.

$$\frac{dN}{dE} = N_0 \left(\frac{E}{E_0} \right)^{\gamma} \tag{3.1}$$

The Vela pulsar

The SED for the Vela pulsar is shown in figure 3. The yellow line is the 3FGL model and its extrapolation below 100 MeV (dashed yellow line). The 3FGL spectrum was derived using 4 years of Pass 7 reprocessed SOURCE data and energy dispersion was not taken into account in the fit. The blue points are found as a result of the GaRDiAn analysis with energy dispersion. As a comparison the cyan line show the result of a "conventional" Science-Tool analysis of 6 years of Pass 8 SOURCE data with a zenith cut at 80 deg, between 63 MeV and 100 GeV, where the Vela pulsar was the only free source, the other sources being fitted using OFF-pulse. The Science-Tool analysis also used energy dispersion and was used to derived the systematics on the GaRDiAn analysis. Once the systematics are taken into account one can see that the 3 analysis: 3FGL, GaRDiAn and Science-Tools are compatible. The COMPTEL points from [7] are also reported on figure 3. All 3 *Fermi*-LAT analysis seems to undershoot those points.

The Crab pulsar and nebula

The SED for the Crab pulsar and nebula system is shown in figure 4, compared to the 3FGL model which was fitted to 4 years of Pass 7 reprocessed SOURCE data with energy $\geq$ 100 MeV (yellow line). It is superposed to the points obtained with this analysis (blue points) and points coming from observations by COMPTEL of the Crab nebula [4] (green bars). As one can see, the LAT data appear to be in agreement with the COMPTEL measurements. The systematics on the GaRDiAn analysis used for the Crab are the same as the one derived from Vela.

Conclusion

Pass 8 increased effective area provides more photons at low energy and Pass 8 event classes and new energy dispersion function provides tools that make analysis under 100 MeV tantalising.The analysis shown here uses GaRDiAn full-sky fit capacities to conduct a first analysis of the Fermi-LAT sky under 100 MeV using the new Pass 8 data set, focussing on two well known sources, Vela and the Crab. The results shows agreement with the 3FGL study (above 100 MeV) once we account for systematics errors.

Acknowledgments

The *Fermi*-LAT Collaboration acknowledges support from a number of agencies and institutes for both development and the operation of the LAT as well as scientific data analysis. These include NASA and DOE in the United States, CEA/Irfu and IN2P3/CNRS in France, ASI and INFN in Italy, MEXT, KEK, and JAXA in Japan, and the K. A. Wallenberg Foundation, the Swedish Research Council and the National Space Board in Sweden. Additional support from INAF in Italy and CNES in France for science analysis during the operations phase is also gratefully acknowledged.

This work has been carried out thanks to the support of the OCEVU Labex (ANR-11-LABX-0060) and the A*MIDEX project (ANR-11-IDEX-0001-02) funded by the "Investissements d'Avenir" French government program managed by the ANR.

References

[1] Atwood, W. B et al., *Pass 8: Toward the Full Realization of the Fermi-LAT Scientific Potential*, *Fermi Symposium 2012 Procs.* (**2012**) [arXiv:1303.3514]

[2] Atwood, W. B. et al., *The Large Area Telescope on the Fermi Gamma-Ray Space Telescope Mission*, The *Astrophysical Journal* 697(2), 1071 (**2009**).

[3] The Fermi-LAT Collaboration, *Fermi Large Area Telescope Third Source Catalog*, (**2015**), arXiv:1501.02003 [astro-ph.HE]

[4] Kuiper L. et al. *The Crab pulsar in the 0.75–30 MeV range as seen by CGRO COMPTEL*, *Astronomy and Astrophysics* 378, 918, (**2001**)

[5] Ackermann et al. *Fermi-LAT observation of the diffuse γ-ray emission: Implications for cosmic rays and the interstellar medium*, *Astronomy and Astrophysics* 750, (**2012**)

[6] Ackermann et al. *The Fermi Large Area Telescope On Orbit: Event Classification, Instrument Response Functions, and Calibration*, *The Astrophysical Journal Supplement Series* 203 4 (**2012**)

[7] Kuiper & Hermsen, *The soft gamma-ray pulsar population: an high-energy overview*, *arXiv:1502.06769* (**2015**)

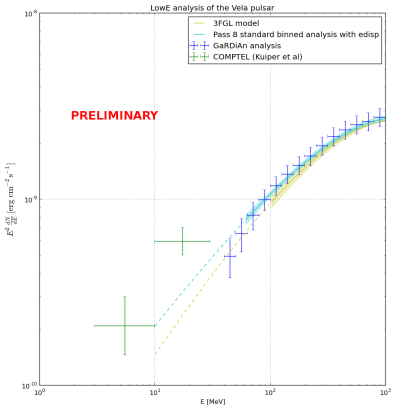

Figure 3: Spectral energy distribution for the Vela pulsar. The blue points have been derived from this analysis while the yellow line is the 3FGL model. The cyan line is the result of the fit of a power-law with super exponential cut-off with the Science-Tools on the range 63 MeV - 100 GeV. The green points shows COMPTEL measurement form [7].

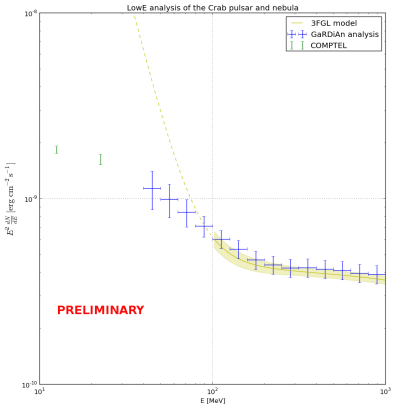

Figure 4: Spectral energy for the Crab, the blue points have been derived from this analysis while the green points are from COMPTEL Crab nebula SED [4] (the dominent component at low energy).The green bars are 1σ statistical error. The other line shows the 3FGL model.